Available online at www.sciencedirect.com
ScienceDirect
Catalysis Today 123 (2007) 104–112
CATALYSIS TODAY
www.elsevier.com/locate/cattod

Photochemical synthesis of oligothiophene thin films and nano-patterns in condensed multilayer films of 2,5-diiodothiophene—Effects of surface chemistry of substrates

Seong H. Kim *, Sudarshan Natarajan [1], Guangming Liu [2]

Department of Chemical Engineering, Pennsylvania State University, University Park, PA 16802, USA

Available online 13 March 2007

Abstract

This paper reviews photochemical reactions of 2,5-diiodothiophene multilayers on various solid substrates that lead to production of oligothiophene thin films and micro-patterns with a thickness relevant to nanotechnology applications. Upon UV absorption, the C–I bond of 2,5-diiodothiophene dissociates generating a thienyl radical and iodine atom. The radicals generated in multilayers can react with other radicals or intact monomers to form dimers. Since the C–I bonds are present at the ends of the coupling reaction product, further photodissociation and coupling reactions can take place forming oligomeric species. On inert substrates, the average conjugation length of the product is about 3–4 thienyl units. Various pattern generation schemes can be incorporated with this photochemical reaction. Examples of masked irradiation, wettability pre-patterning, and controlled clustering of thermal desorption process are demonstrated. On copper surfaces, the average conjugation length of the produced oligothiophene is increased to 6–7 units, which is long enough for technical applications. This increase is due to Ullmann coupling reactions at the buried interface between the copper and adsorbed film. The mechanism for this buried surface reaction is elucidated from the thickness dependence of the conjugation length and Ullmann coupling side product.

Keywords: Nanotechnology; Oligothiophene thin films; Photochemical reaction

1. Introduction

Surface reactions are of great interests from both a fundamental and industrial point of view. Fundamental studies on well-controlled surfaces in ultra-high vacuum conditions provide molecular details into surface reaction dynamics and mechanisms. Heterogeneous catalytic reactions are widely used in industrial processes to produce many specialty compounds as well as commodity chemicals. Most surface reactions can be categorized into four classes shown in Fig. 1. In Fig. 1a, reactant molecules adsorb on the surface and undergo reactions at the surface, and product molecules desorb from the surface regenerating reactive surface sites. This is the case of most heterogeneous catalytic reactions [1]. If the products are not desorbed, the surface reaction stops once the reaction product completely covers the surface. In Fig. 1b, reactant molecules diffuse into the surface and reaction occurs in the subsurface. Oxidation and corrosion of metals are typical examples of this category. In Fig. 1c, reactive species are generated in the gas phase and reactions occur at the interface between the gas and the deposited film. In some cases, reactive species are generated photochemically in the deposited film, causing reactions in the film. Although it can have some physical influences in the film growth, the substrate is not involved directly in chemical reactions at the interface. Typical examples of this category include physical/chemical vapor deposition of thin films or photolithography of resist films. In Fig. 1d, reactants diffuse through the growing product film to the substrate surface and the reaction occurs at the film-substrate interface. Surface reactions of this kind are catalytic polymerizations such as the Ziegler–Natta olefin polymerization [2].

Recently, reactions in thick multilayers (Fig. 1c) are receiving considerable attention due to their potential applications to *in situ* fabrication of functional organic structures on

* Corresponding author. Tel.: +1 814 863 4809; fax: +1 814 865 7846.
E-mail address: shkim@engr.psu.edu (S.H. Kim).
[1] Present address: Lam Research Corp., Fremont, CA 94538, USA.
[2] Present address: Department of Materials Science and Engineering, University of Delaware, Newark, DE 19716, USA.

0920-5861/$ – see front matter © 2007 Elsevier B.V. All rights reserved.
doi:10.1016/j.cattod.2007.01.065

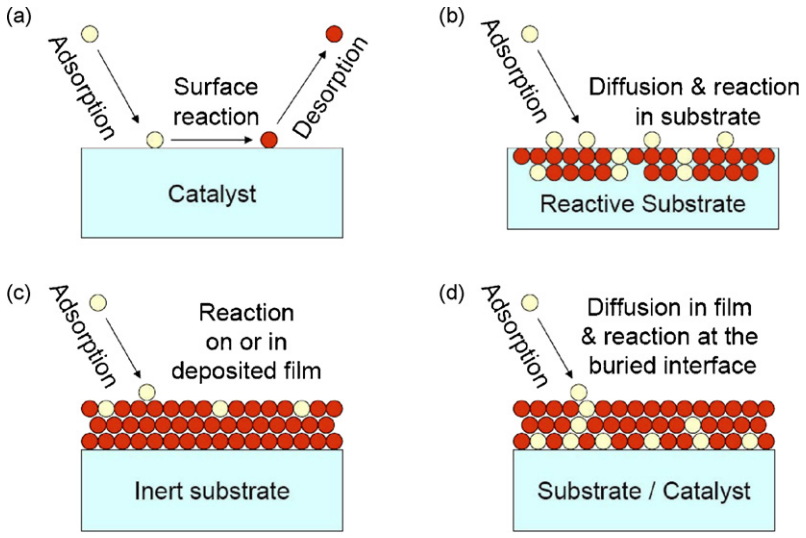

Fig. 1. (a–d) Four types of surface reactions involved in various catalytic reactions and thin film growth processes.

device surfaces [3,4]. A specific interest is given to the possibility of producing conjugated polymer structures *via* non-thermal reactions in multilayers of the monolayer species adsorbed or condensed on the substrate surface [5–18]. These non-thermal multilayer reactions can produce conjugated polymer thin films and micro-patterns that are difficult to generate in conventional ways due to the intractability of conjugated polymers without solubilizing side chain groups.

An alternative and more challenging, but more promising, approach is to apply organo-metallic reactions to growth of conjugated polymer thin films and micro-patterns directly on the substrate surface from the monomer (Fig. 1d). One of the most widely used methods for synthesis of conjugated polymers is the Ullmann aryl-aryl coupling reaction [19,20]. On copper surfaces, aryl halide compounds dissociate and undergo aryl-aryl coupling reactions [21–26]. This thermally activated reaction can produce only submonolayer-thick dimer molecules in the absence of proper solvents. This is because desorption or dissolution of iodine-containing species without solvents are difficult at the reaction temperature. In order to attain conjugated polymer films and micro-patterns which are thick enough for technical applications (for example, 10–100 nm), one must be able to continuously remove reaction products for regeneration of active copper site and supply reactants to the active copper site in a spatially localized monomer film deposited on an active metal substrate.

This paper reviews photochemical reactions of 2,5-diiodothiophene multilayers and the effects of reaction conditions and substrate surface chemistry in generation of oligothiophene patterns and control of the degree of conjugation [27–32]. In this process, a thick film of 2,5-diiodothiophene is deposited on various substrates (such as glass, polyethylene, SiO_2, Au, and Cu) and is activated photochemically with UV at room temperature. 2,5-Diiodothiophene is solid at room temperature (m.p. 34 °C), so it can be vapor deposited by simple evaporation. The use of photo-activation avoids the need for thermal activation, so the monomer film can be kept adsorbed at the surface long enough for chemical reactions to occur. The reaction products are identified as oligothiophene with various characterization techniques. Since photochemical reactions are involved in this process, oligothiophene micro-patterns can easily be generated by irradiating UV light through a photomask (Fig. 1c). Micro-patterns can also be generated without using the photomask if the wetting/non-wetting behaviors of 2,5-diiodothiophene species are controlled during the process (Fig. 1c). The degree of conjugation length is much longer for reactions on copper (Fig. 1d) than those on other chemically inert surfaces (Fig. 1c).

2. Photochemical synthesis and patterning processes

The 2,5-diiodothiophene precursor can be deposited on a substrate held at room temperature by physical vapor deposition from a heated evaporation source in Ar ambient. Glass, silicon wafer and gold substrates can be cleaned with any standard cleaning methods. For copper, a 1.5N nitric acid treatment prior to use works well to remove oxide layers as well as organic contaminants. Since the photochemical process involves radical generation, it is important to do UV irradiation in oxygen-free environments. In ambient conditions, the deposited monomer film should be irradiated with a collimated UV beam from a high-pressure Hg lamp in argon. In UHV conditions, UV can be irradiated during the precursor dose on the substrate cooled at ~100 K. The IR radiation from the UV lamp must be removed using a water filter to prevent the substrate temperature rise. The UV power can be controlled between 40 and 200 W, depending on experimental conditions. If needed, unreacted precursors after UV irradiation are removed by washing with hexane or by heating in UHV. For micro- and submicro-pattern generations, several different strategies can be applied: UV irradiation through a photomask, wettability patterning of the substrate, and clustering during temperature-programmed desorption of unreacted precursors in UHV. More details can be found in the previous publications [27–32].

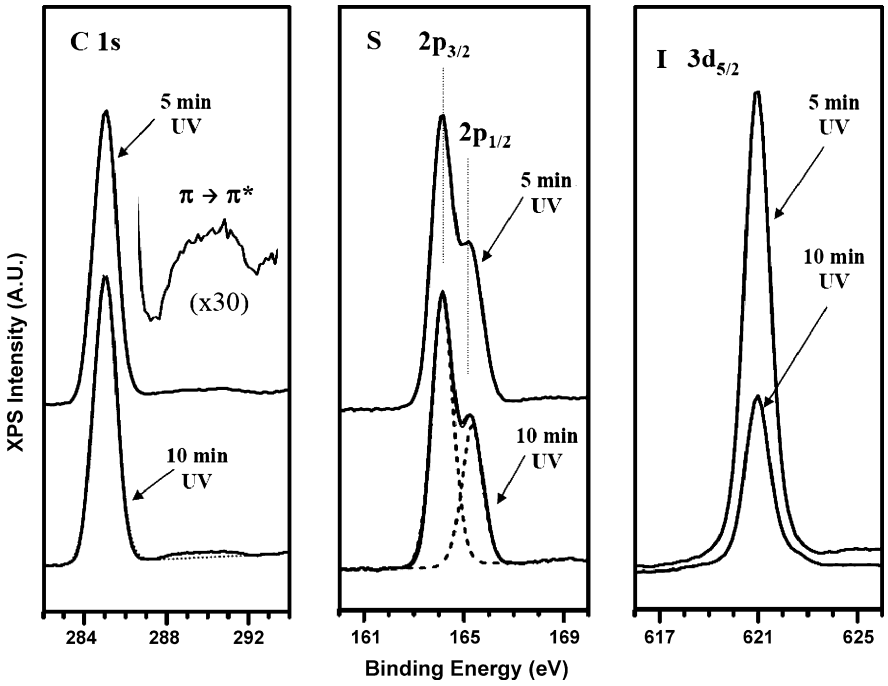

Fig. 2. High-resolution XPS of C 1s, S 2p, and I 3d region for the oligothiophene film produced by 5 and 10 min UV irradiation on 2,5-diiodothiophene film [27].

3. Photochemical reaction products on chemically inert substrates (glass, SiO_2, Au)

The photochemical reaction products can be analyzed with X-ray photoelectron spectroscopy (XPS), infrared and Raman spectroscopy, near-edge X-ray absorption fine structure (NEXAFS), and photoluminescence (PL) spectroscopy. The results from these analyses are summarized in this section.

The well-established photodissociation mechanism of iodo-organic compounds supports the selective dissociation of the C–I bond of the iodothiophene molecule upon absorption of UV photons (λ = 250–300 nm) generating a thienyl radical and an iodine atom [33,34]. This can clearly be seen in XPS (Fig. 2) [27]. The intensity of I $3d_{5/2}$ peak at 620.8 eV, corresponding to the iodothiophene group, decreases as the UV irradiation time increases. The C region shown in Fig. 2 displays two components—the C 1s peak at 285 eV and the broad shake-up transition in the range of 287.5–292.5 eV. The binding energy difference of the α and β carbons in thiophene is only 0.34 eV, which is smaller than the resolution of our XPS instrument [35]. There are no other carbonaceous species detected in XPS, suggesting the homogeneity of carbon species. The shake-up peak originates from π–π^* transitions between highest occupied molecular orbital (HOMO) and lowest unoccupied molecular orbital (LUMO) of the conjugated polymer backbone [35]. The S 2p XPS region in Fig. 2 shows a well-resolved spin-orbit doublet peak at 164.1 eV ($2p_{3/2}$) and 165.3 eV ($2p_{1/2}$). Their positions are consistent with the reported values for polythiophene [35]. The average S/C atomic ratio is found to be around 0.24, which is in agreement with the theoretical value of 0.25. These results indicate that the C–S bond in the thienyl ring is preserved during the photochemical process.

The growth of oligothiophene species through photochemical reactions of 2,5-diiodothiophene can be observed with IR (Fig. 3) [27]. The peak positions of the C–C symmetric and asymmetric stretching vibrations can be used as a probe for oligomer or polymer formation. The 2,5-diiodothiophene precursor has peaks at 1388 cm^{-1} (sym) and 1497 cm^{-1} (asym), while the polythiophene has peaks at 1440 cm^{-1} (sym) and 1490 cm^{-1} (asym) [36–38]. In the case of UV-irradiated precursor film, three distinct changes can be observed: (a) a gradual shift of the C–C symmetric peak from 1388 cm^{-1} to higher wave numbers, (b) a peak growth at 1430 cm^{-1}, and (c) a significant growth of the 1492 cm^{-1} peak intensity. These changes are characteristic of α-coupled oligothiophene growth from precursors [36,38]. The two peaks at 1345 and 1200 cm^{-1} can be attributed to a trace amount of iodine-doping inside the film [39]. Once again, the intactness of the monomer structure can be confirmed with the absence of peaks at 3060–3125 cm^{-1} which correspond to the hydrogen at the β positions in the

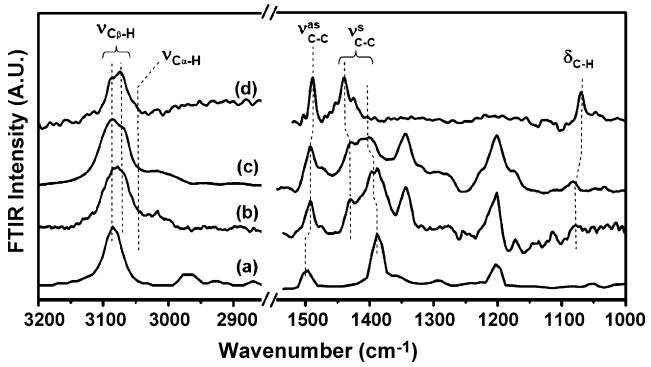

Fig. 3. IR spectra of: (a) 2,5-diiodothiophene, (b) oligothiophene film produced by 2 min UV irradiation, (c) oligothiophene film produced by 5 min UV irradiation, and (d) chemically synthesized polythiophene [27].

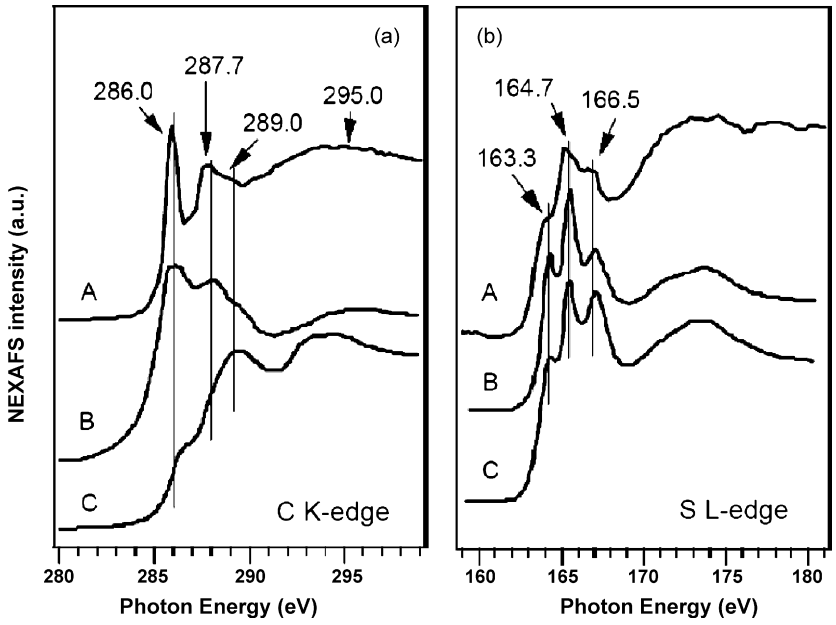

Fig. 4. (a) C K-edge and (b) S L-edge spectra of grazing incidence NEXAFS for photochemically synthesized oligothiophene film (A), electrochemically deposited polythiophene film (B), and electrochemically deposited poly-3-dodecyl-thiophene film (C) [29].

thienyl group [38]. A very weak shoulder at 3020 cm^{-1} might be assigned to the C-H stretching at the α position in the thienyl group due to a small degree of mis-linking in the oligomer [40].

The NEXAFS spectra of the photosynthesized film provide additional evidence for the structural integrity of the thienyl ring in the produced oligothiophene species. Fig. 4 displays grazing incidence NEXAFS spectra of the carbon K-edge and sulfur L-edge regions of the photochemically synthesized film on a Au film [29]. In the carbon K-edge region, there are two sharp transition peaks at 286.0 and 287.7 eV, one shoulder peak at 289.0 eV, and one broad transition at 295.0 eV. These peak positions are in good agreement with the theoretical calculation and other experimental data for polythiophene and poly-3-dodecyl-thiophene [41–43].

It should be noted that there is no discernible peak around 292.5 eV in the carbon K-edge originating from the σ^* (C–C) resonance of alkyl chains [43]. The sulfur L-edge shows characteristic peaks of polythiophene at 163.3, 164.7, and 166.5 eV [43].

The PL excitation and emission spectra of the photochemically synthesized films are shown in Fig. 5 [27]. The presence of strong photoluminescence emission with a maximum at 545 nm and a long tail up to 650 nm clearly indicates the presence of oligothiophene. From the maximum peak position, it is inferred that the most dominant species in the film are α-connected oligomers of ∼4 thienyl monomer units.

4. Generation of oligothiophene micro- and submicro-patterns

4.1. UV irradiation through a photomask

The direct photochemical synthesis can be easily incorporated with the conventional photolithography process to make micro-patterns *via* region-selective direct conversion of the precursor multilayer film adsorbed on the substrate to the polymer (Fig. 6a) [27,29]. The tapping mode atomic force microscopy (AFM) revealed that the surface of the produced film is very smooth. The root-mean-square roughness calculated over a 5 μm × 5 μm area was about 2 Å [27]. The same photochemical pattern generation of oligothiophene can be applied to inert polymer surfaces (such as polyethylene) as long as the precursor wets the substrate surface. The photomask approach can also be applied to the deposition process in UHV [29].

4.2. Mask-less patterning via selective deposition of precursors on chemically modified substrates

The mask-less patterning approach utilizes selective aggregation of molecules on chemically heterogenized substrate surfaces

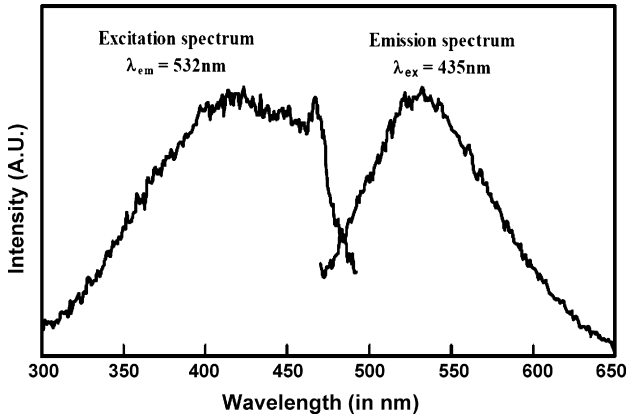

Fig. 5. Photoluminescence excitation and emission spectra of the photochemically synthesized oligothiophene films on a glass substrate [27].

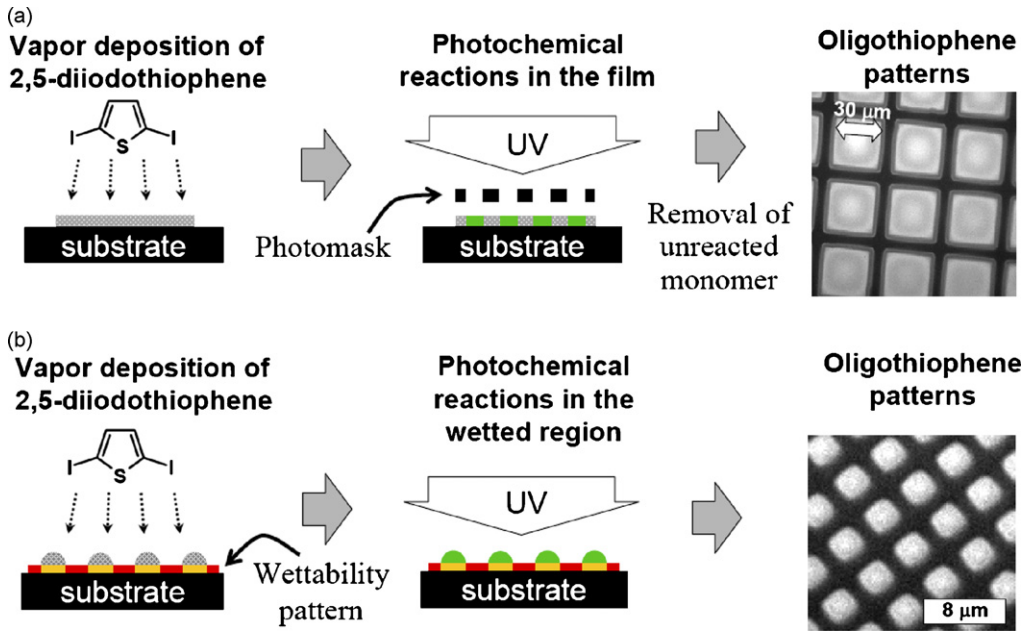

Fig. 6. (a) Micro-patterning by UV irradiation through a photomask. (b) Mask-less micro-patterning by selective adsorption on wettability patterned substrate [27–29].

containing periodic arrays of wettable regions surrounded by non-wettable regions. The wettability-patterned substrates have been utilized for selective condensation of liquids or selective dewetting of polymer thin films [44–56]. The same principle can be utilized for production of conjugated polymer patterns if the following conditions are met [28]. First, the precursor molecules on the substrate should have enough mobility so they can migrate until they find the minimum energy regions provided by preferable surface wettability or intermolecular interactions. This condition seems to be met easily since the substrate temperature (~25 °C) during the precursor deposition is very close to the melting temperature of the precursor (34 °C). Second, there should be proper chemical modifiers that will generate a high enough wettability contrast for selective aggregation of precursor molecules on the substrate.

In the case of 2,5-diiodothiophene on gold, 2-mercaptothiophene can be used to create the wetting region. 2,5-Diiodothiphene readily wet the thiophene-terminated monolayer surface. The non-wetting region can be coated with 1-hexadecanethiol self-assembled monolayer (SAM). Various SAM patterns can be created easily using a stamping technique (Fig. 6b) [44]. One limitation of the wettability-based pattern generation of oligothiophene is that the width of the less wettable regions between the more wettable regions should be smaller than the spinodal wavelength (characteristic length scale of dewetting) of the film on a homogeneous substrate [56]. Otherwise, the fidelity of the wettability pattern recognition decreases.

4.3. Clustering of unreacted precursors during TPD in UHV

In UHV, the thermal desorption of 2,5-diiodothiophene multilayers exhibits complicated desorption behaviors deviating from simple zeroth order desorption kinetics [57–60]. Fig. 7 displays temperature programmed desorption (TPD) profiles of 2,5-diiodothiophene multilayers deposited on gold at 100 K [32]. The 2,5-diiodothiophene molecule decomposes almost completely on clean gold surface. After complete passivation of the gold surface, the first multilayer desorption peak grows at ~220 K with a broad and rather symmetric shape. As the multilayer thickness is increased, a second peak grows at ~235 K. The second peak grows faster than the first peak and eventually becomes dominant at high doses. The desorption

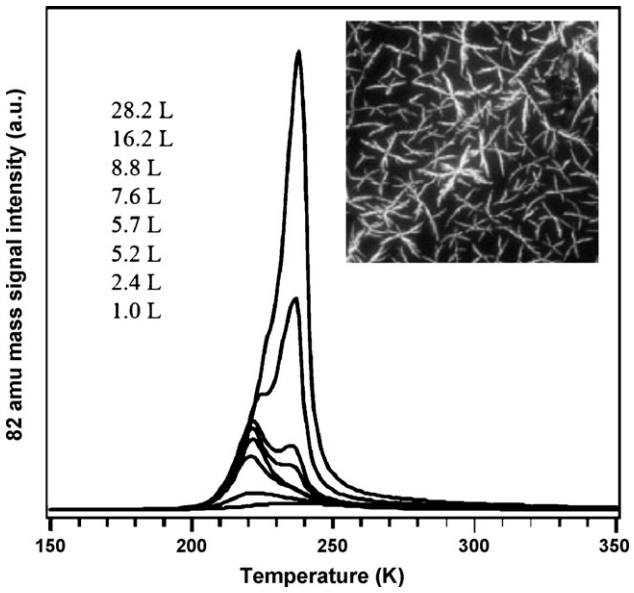

Fig. 7. TPD profile of 2,5-diiodothiophene multilayers adsorbed on gold at 100 K. The inset shows a fluorescence microscope image of oligothiophene produced by UV irradiation during 2,5-diiodothiophene adsorption at 100 K followed by slow heating to room temperature [32].

profile of the second peak is slightly asymmetric at the peak position, following zeroth order desorption kinetics. These changes are due to a lateral clustering of adsorbed molecules during TPD [61].

This clustering phenomenon can be used to create submicro-scale features of oligothiophene species [32]. For this purpose, a small fraction of 2,5-diiodothiophene precursor molecules is converted to oligothiophene species at low temperature and then the unreacted of precursor multilayer film is heated slowly. At a low concentration of the oligothiophene species produced, plus-shaped dendritic fibers are exclusively formed. When the surface coverage of oligothiophene species is slightly increased, short branches are formed on the side of long fibers, producing a feather-like shape (Fig. 7, inset). As the oligothiophene concentration is further increased, the produced patterns progress to highly curved multi-fiber aggregates and eventually almost completely covered patches.

The direction of the oligothiophene fibrils can be controlled using topographic patterns on the substrate. The feasibility of this approach is demonstrated in Fig. 8 [32]. An array of parallel trench lines (~70 nm wide, ~200 nm deep, ~30 μm long) are produced in a PMMA photoresist film and coated with a 10 nm thick gold film (Fig. 8a). On this substrate, oligothiophene is produced photochemically during the deposition of 2,5-diiodothiophene multilayer and allowed to aggregate during the desorption of the unreacted 2,5-diiodothiophene. Fig. 8b exhibits the fluorescence micrograph image of the produced oligothiophene fibers on and around the nano-trench array. A high degree of alignment can be seen for oligothiophene fibers grown on the nano-trench array region, while the fibers grown on the flat region (outside the nano-trench array) are highly branched and randomly oriented. This demonstration may open up new ways of growing conjugated polymer fibers with controlled alignments. By combining the surface morphology and/or chemistry control methods with the photolithography technique, one could accomplish a higher level of spatial control.

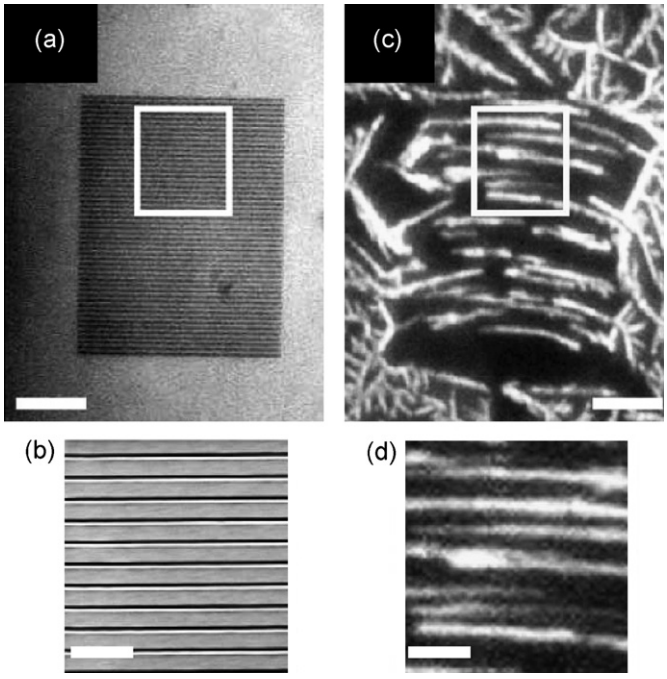

Fig. 8. (a) Optical microscope image of an array of trenches (width = 70 nm, depth = 200 nm, length = 30 μm) made by imprinting a PMMA resist film followed by 10 nm thick gold deposition. (b) Field-emission scanning electron microscope image of the marked region in 'a'. (c) Fluorescence microscope image of oligothiophene nanofibers on and around the nano-patterned substrate region. (d) Enlarged fluorescence microscope image of the parallel oligothiophene fibers in the marked region in 'c'. The scale bar in 'a' and 'c' is 10 μm. The scale bar in 'b' and 'd' is 2 μm [32].

5. Increased conjugation length through photo-assisted Ullmann coupling reactions at the buried Cu-film interface

If the substrate metal is actively involved for Ullmann coupling reactions during the photochemical process, the produced film can have longer conjugation lengths, emitting longer wavelength PL. The PL spectrum of the 100 nm thick film synthesized on Cu is peaked at ~605 nm (orange red), while those of the films with the same thickness synthesized on other substrates are at ~545 nm (greenish yellow) [30]. The difference in the conjugation length can also be detected with Raman spectroscopy as shown in Fig. 9 [30]. It is known that as the number of conjugated thiophene ring units increases from 3 to 8, the C_α=C_β asymmetric stretching peak location gradually shifts from 1530 to 1502 cm^{-1} and the I_{asym}/I_{sym} intensity ratio decreases gradually from ~1 to ~0.2 [37,38]. For the oligothiophene film synthesized on Au, the C_α=C_β symmetric and anti-symmetric peaks are located at 1440 and 1520 cm^{-1}, respectively, and the I_{asym}/I_{sym} ratio is ~1. For the oligothiophene film synthesized on Cu, the ring symmetric peak is at ~1450 cm^{-1} and the C_α=C_β asymmetric peak appears as a shoulder at ~1510 cm^{-1}. The I_{asym}/I_{sym} intensity ratio is ~0.30. Therefore, the average conjugation length of the oligothiophene synthesized on Au is estimated as 3–4 and that

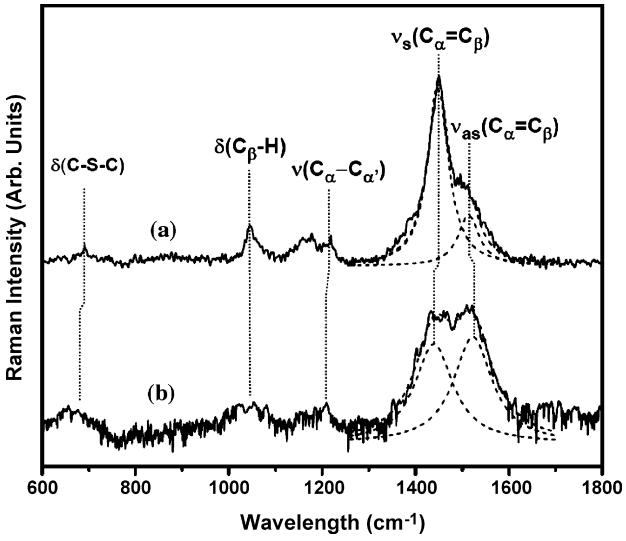

Fig. 9. Surface-enhanced Raman spectra of oligothiophene film photochemically synthesized from 2,5-diiodothiophene film deposited on: (a) Cu and (b) Au [30].

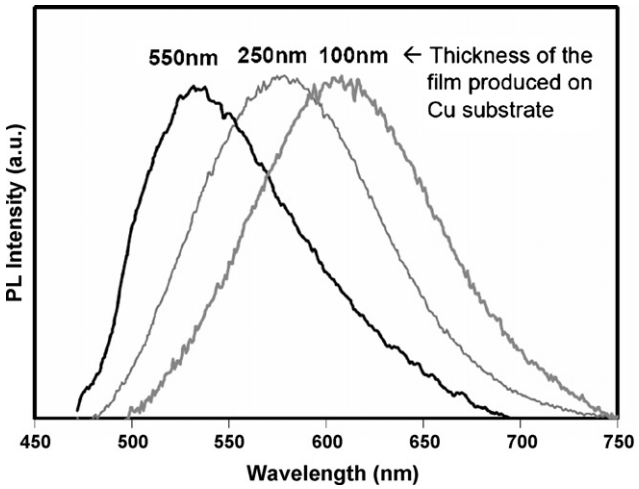

Fig. 10. Photoluminescence (PL) emission spectra of oligothiophene films produced photochemically on copper with three different thicknesses −100, 250, and 550 nm [31].

on Cu is 6–7. These results clearly indicate that there are copper-mediated Ullmann coupling contributions in the photochemical conversion of 2,5-diiodothiophene to oligothiophene (Fig. 1d).

The average conjugation length of the oligothiophene film produced on copper depends on the film thickness [31]. Fig. 10 compares the PL spectra of oligothiophene films of three different thicknesses (∼100, ∼250, and ∼550 nm) produced on copper substrates. The PL emission maxima of the 100 and 250 nm thick films show significant red-shift compared to that of the 550 nm thick film. The conjugation length estimated from the PL maximum is ∼7 for the 100 nm thick film, 4–5 for the 250 nm thick film, and 3–4 for the 550 nm thick film [62]. These results imply that the Ullmann coupling contribution decreases as the film thickness increases.

The Cu-mediated Ullmann coupling of 2,5-diiodothiophene produces copper iodide (CuI) as a by-product, which can be used as a signature of the Ullmann coupling reaction. Fig. 11 compares the I $3d_{5/2}$ XPS and Cu $L_3M_{4,5}M_{4,5}$ Auger peaks for three different thickness oligothiophene films (100, 250, and 550 nm) produced on copper [31]. In the I $3d_{5/2}$ XPS region, the peak at 620.7 eV is from the iodine covalently bonded to carbon and the peak at 619.7 eV is from the iodide anion in CuI [63,64]. As the film thickness increases, the CuI peak decreases at 619.7 eV and the C–I peak increases at 620.7 eV. For the 550 nm film, the CuI portion disappears almost completely and all the detected iodine species is ascribed to the unreacted C–I bond of short conjugation length oligomers. The same trend can be seen for the Cu $L_3M_{4,5}M_{4,5}$ Auger peak region—the decrease of CuI (916.1 eV) with the increase of the film thickness. The Cu/I ratio is around 1, indicating the stoichiometry of CuI. There is no metallic Cu substrate peak at 918.5 eV or CuS and Cu_2S species at 917 eV detected for all thicknesses [63,65].

The fact that CuI species is detected for films much thicker than the photoelectron escape depth (typically 2–3 nm) provides a very important clue for understanding the reaction process. This indicates that the CuI species are distributed throughout the entire film. CuI is not soluble in thiophene or 2-iodothiophene liquid. If the CuI species is produced at the substrate/film interface, it will be accumulated beneath the film and not be detected in XPS. In addition, the accumulation of CuI at the substrate/film interface will stop the Ullmann coupling reaction after completion of one or a few monolayer thick CuI layer formations. Ruling out the CuI dissolution and diffusion during the photochemical reaction, the diffusing species must be the thienyl-copper intermediates formed by the reaction of the photogenerated thienyl radical with the copper atom at the substrate surface. The reaction of the thienyl-copper intermediate with iodothiophene produces the C–C bond between the thiophene units and CuI as a by-product.

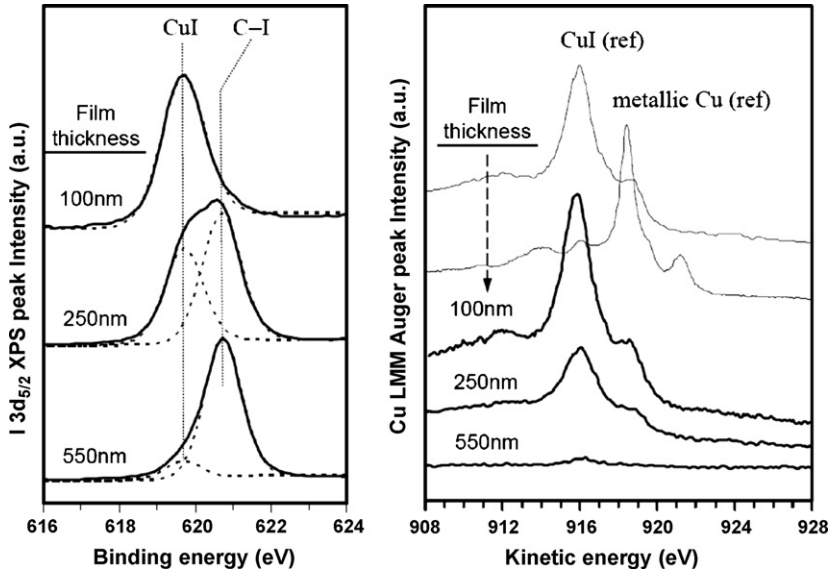

Fig. 11. High resolution XPS data of the I $3d_{5/2}$ and Cu $L_3M_{4,5}M_{4,5}$ Auger regions for oligothiophene films produced photochemically on copper with three different thicknesses −100, 250, and 550 nm [31].

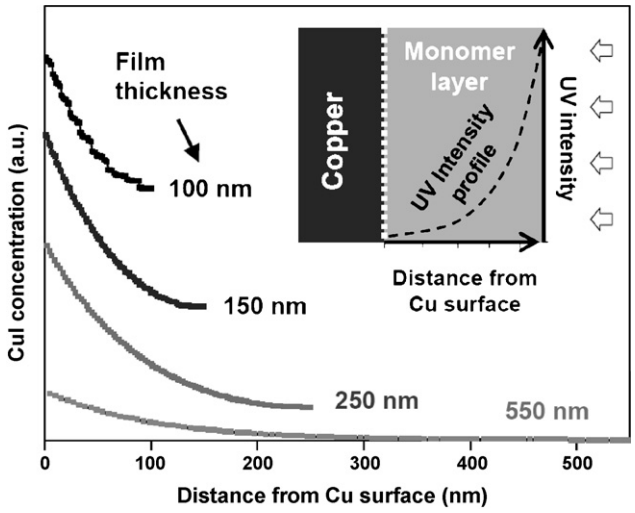

Fig. 12. Numerical simulation results of one-dimensional diffusion-reaction model capturing the effect of monomer film thickness on the extent of contribution of Ullmann coupling reaction. See texts for simulation details. The inset shows a schematic view of the photon flux distribution in the deposited 2,5-diiodothiophene film [31].

The thickness dependence of the Ullmann coupling contribution is related to the decrease of the UV light intensity reaching at the film-copper interface where the thienyl-copper intermediate species is produced [31]. The concentration of the intermediate species is determined by the UV photon intensity reaching the copper/film interface. Since UV photons are absorbed by the monomer molecules, the UV flux decreases exponentially as it travels through the film (Fig. 12, inset). The generation, reaction, and diffusion of reactive species at the Cu/film interface can be simulated using a steady state diffusion-reaction kinetic model [66]. In this simulation, the diffusion rate of the thienyl-copper intermediate species is assumed to be comparable to the reaction rate of the intermediate species with the iodothiophene species. When the 2,5-diiodothiophene precursor film is irradiated with UV light, a liquid phase is formed transiently in the precursor film before the entire film gets solidified due to accumulation of oligothiophene molecules with only one iodine atom such as 2-iodothiophene which is liquid at room temperature. This liquid phase can facilitate the dissolution and diffusion of the thienyl-copper intermediate species, as in the conventional solution phase process.

Fig. 12 plots the simulated CuI concentration profile as a function of the distance (l) from the copper surface for the initial 0.1 s period for various monomer film thicknesses (L) [31]. For the numerical simulation purpose, the diffusion constant of the thienyl-copper intermediate in the film (D) is assumed to be 10^{-6} cm^2/s [66] and the rate constant (K) of the reaction between thienyl-copper species and monomer (or oligomers) is assumed to be an order of D/L^2 for L = 100 nm. The simulation results are qualitatively consistent with the experimental observations. The CuI concentration at the copper surface decreases rapidly with the increase of the monomer film thickness. Therefore, the Ullmann coupling contribution during the photochemical reaction decreases with the film thickness.

6. Conclusions

Photochemical reactions of precursor molecule multilayers on solid substrate surfaces can be utilized for production of thin films of conjugated oligomers and polymers with a thickness relevant to nanotechnology applications. Since the conjugated organic molecules are produced *via* photochemical reactions, the use of photomasks allows micro-pattern generation of any arbitrary shapes. Arrays of micro-patterns with a certain periodicity can be produced by combining the photochemistry with selective aggregation of precursors on a wettability-patterned substrate surface. Aligned nanofibers of conjugated molecules can be produced by controlling the clustering behavior during the thermal desorption of unreacted precursor layers containing photochemical reaction products. The conjugation length of the produced molecules is strongly dependent on the reactivity of the substrate and the regeneration of reactive surface sites during the photochemical reactions.

Acknowledgements

This work is supported by the Petroleum Research Foundation (Grant No. 40605-G5), the National Science Foundation (Grant No. DMI-0210229), and the 3M Nontenured Faculty Award.

References

[1] S.C. Street, C. Xu, D.W. Goodman, Annu. Rev. Phys. Chem. 48 (1997) 43.
[2] S.H. Kim, G.A. Somorjai, Proc. Natl. Acad. Sci. U.S.A. 103 (2006) 15289.
[3] H. Meng, D.F. Perepichka, M. Bendikov, F. Wudl, G.Z. Pan, W. Yu, W. Dong, S. Brown, J. Am. Chem. Soc. 125 (2003) 15151.
[4] H. Meng, D.F. Perepichka, F. Wudl, Angew. Chem. Int. Ed. 42 (2003) 658.
[5] J.E. Hernandez, H. Ahn, J.E. Whitten, J. Phys. Chem. B 105 (2001) 8339.
[6] J. Bai, C. Snively, W.N. Delgass, J. Lauterbach, Adv. Mater. 14 (21) (2002) 1546.
[7] M.E. Ryan, A.M. Hynes, S.H. Wheale, J.P.S. Badyal, C. Hardacre, R.M. Ormerod, Chem. Mater. 8 (1996) 916.
[8] L.M.H. Groenewoud, G.H.M. Engbers, J.G.A. Terlingen, H. Wormeester, J. Feijen, Langmuir 16 (2000) 6278.
[9] P. Haaland, J. Targove, Appl. Phys. Lett. 61 (1992) 34.
[10] T. Iyoda, M. Kitano, T. Shimidzu, Chem. Commun. (1991) 1681.
[11] S. Nishio, S. Okada, Y. Minamimoto, M. Okumura, A. Matsuzaki, H. Sato, J. Photochem. Photobiol. A: Chem. 116 (1998) 245.
[12] C. Wochnowski, S. Metev, Appl. Surf. Sci. 186 (2002) 34.
[13] W.R. Salaneck, C.R. Wu, J.O. Nilsson, J.L. Bredas, Synth. Met. 21 (1987) 57.
[14] T.A. Land, J.C. Hemminger, Surf. Sci. 268 (1992) 179.
[15] H. Raza, P.L. Wincott, G. Thornton, R. Casanova, A. Rodriguez, Surf. Sci. 390 (1997) 256.
[16] A. Nambu, H. Kondoh, I. Nakai, K. Amemiya, T. Ohta, Surf. Sci. 530 (2003) 101.
[17] K.M. Baumgärtner, M. Volmer-Uebing, J. Taborski, P. Bäuerle, E. Umbach, Ber. Bunsen-Ges. Phys. Chem. 95 (1991) 1488.
[18] S. Tepavcevic, Y. Choi, L. Hanley, J. Am. Chem. Soc. 125 (2003) 2396.
[19] R.D. Rieke, Science 246 (1989) 1260.
[20] A. Fürstner, Angew. Chem. Int. Ed. Engl. 32 (1993) 164.
[21] M. Xi, B.E. Bent, J. Am. Chem. Soc. 115 (1993) 7426.
[22] M. Xi, B.E. Bent, Langmuir 10 (1994) 505.
[23] D.W. Kash, D.H. Sun, M. Xi, G.W. Flynn, B.E. Bent, J. Phys. Chem. 100 (1996) 16621.
[24] J.M. Meyers, A.J. Gellman, Surf. Sci. 337 (1995) 40.

[25] D. Syomin, B.E. Koel, Surf. Sci. 490 (2001) 265.
[26] S.-W. Hla, L. Bartels, G. Meyer, K.-H. Rider, Phys. Rev. Lett. 85 (2000) 2777.
[27] S. Natarajan, S.H. Kim, Thin Solid Films 496 (2006) 606.
[28] S. Natarajan, S.H. Kim, Langmuir 21 (2005) 7052.
[29] G. Liu, S. Natarajan, S.H. Kim, Surf. Sci. 592 (2005) L305.
[30] S. Natarajan, S.H. Kim, Chem. Commun. (2006) 729.
[31] S. Natarajan, G. Liu, S.H. Kim, J. Phys. Chem. B 110 (2006) 8047.
[32] G. Liu, K.B. Rider, W.J. Nam, S.J. Fonash, S.H. Kim, J. Phys. Chem. B 110 (2006) 20197.
[33] M. Dzvonik, S. Yang, R. Bersohn, J. Chem. Phys. 61 (1971) 4408.
[34] F. Elisei, L. Latterini, G.G. Aloisi, M. D' Auria, J. Phys. Chem. 99 (1995) 5365, and references cited therein.
[35] G. Tourillon, Y. Jugnet, J. Chem. Phys. 89 (1988) 1905.
[36] T. Yamamoto, T. Kamijoh, I. Wataru, J. Polym. Sci. Part A: Polym. Chem. 38 (2001) 1642.
[37] G. Louarn, J.P. Buisson, S. Lefrant, D. Fichou, J. Phys. Chem. 99 (1995) 11399.
[38] Y. Furukawa, M. Akimoto, I. Harada, Synth. Met. 18 (1987) 151.
[39] S. Hotta, W. Shimotsuma, M. Taketani, Synth. Met. 10 (1984) 85.
[40] S. Natarajan, S.H. Kim, J. Photochem. Photobiol. A: Chem. 188 (2007) 342.
[41] A.P. Hitchcock, J.A. Horsley, J. Stöhr, J. Chem. Phys. 85 (1986) 4835.
[42] G. Tourillon, C. Mahatsekake, C. Andrieu, G.P. Williams, R.F. Garrett, W. Braun, Surf. Sci. 201 (1988) 171.
[43] A.P. Hitchcock, G. Tourillon, R. Garrett, G.P. Williams, C. Mahatsekake, C. Andrieu, J. Phys. Chem. B 94 (1990) 2327.
[44] A. Kumar, G.M. Whitesides, Science 263 (1994) 60.
[45] H.A. Biebuyck, G.M. Whitesides, Langmuir 10 (1994) 2790.
[46] H. Gau, S. Herminghaus, P. Lenz, R. Lipowsky, Science 283 (1999) 5398.
[47] D.E. Kataoka, S.M. Troian, Nature 402 (1999) 794.
[48] A.M. Higgins, R.A.L. Jones, Nature 404 (2000) 476.
[49] S. Herminghaus, K. Jacobs, K. Mecke, J. Bischof, A. Fery, M. Ibn-Elhaj, S. Schlagowski, Science 282 (2000) 916.
[50] M. Boltau, S. Walheim, J. Mlynek, G. Krausch, U. Steiner, Nature 391 (1998) 877.
[51] G. Nisato, B.D. Ermi, J.F. Douglas, A. Karim, Macromolecules 32 (1999) 2356.
[52] D. Delongchamp, P.T. Hammond, Adv. Mater. 13 (2001) 1455.
[53] A. Sehgal, V. Ferreiro, J.F. Douglas, E.J. Amis, A. Karim, Langmuir 18 (2002) 7041.
[54] K. Kargupta, A. Sharma, Phys. Rev. Lett. 86 (2001) 4536.
[55] K. Kargupta, A. Sharma, Langmuir 18 (2002) 1893.
[56] K. Kargupta, A. Sharma, Langmuir 19 (2003) 5153.
[57] J. Eng Jr., B.E. Bent, B. Fruhberger, J.G. Chen, J. Phys. Chem. B 101 (20) (1997) 4044.
[58] W.X. Huang, J.M. White, J. Phys. Chem. B 108 (16) (2004) 5060.
[59] W.A. Abdallah, A.E. Nelson, Surf. Sci. 585 (1–2) (2005) 113.
[60] T.J. Rockey, M. Yang, H.L. Dai, Surf. Sci. 589 (1–3) (2005) 42.
[61] S.H. Kim, P.C. Stair, E. Weitz, Surf. Sci. 445 (2000) 177.
[62] D. Fichou, C. Ziegler, in: D. Fichou (Ed.), Handbook of Oligothiophenes and Polythiophenes, Wiley-VCH, Weinheim, Germany, 1999.
[63] R.P. Vasquez, Surf. Sci. Spectra 2 (1994) 149.
[64] D. Sloan, Y.M. Sun, H. Ihm, J.M. White, J. Phys. Chem. B 102 (1998) 6825.
[65] S.K. Chawla, N. Sankarraman, J.H. Payer, J. Electron Spectrosc. Relat. Phenom. 61 (1992) 1.
[66] R.B. Bird, W.E. Stewart, E.N. Lightfoot, Transport Phenomena, Wiley, Singapore, 1994.